Annals of Glaciology 33 2001

Sea-ice kinematics measured with GPS drifters

Matti Leppäranta,[1] Zhang Zhanhai,[1,2] Jari Haapala,[1] Tapani Stipa[1,3]
[1]*Department of Geophysics, University of Helsinki, P.O. Box 4 (Fabianinkatu 24 A), FIN-00014 Helsinki, Finland*
[2]*National Research Center for Marine Environment Forecasts, No. 8 Da Hui Si, Hai Dian Division, Beijing, China*
[3]*Finnish Institute of Marine Research, P.O. Box 33, FIN-00931 Helsinki, Finland*

ABSTRACT. A sea-ice dynamics experiment was performed in the Baltic Sea in March 1997. A new type of drifter was constructed based on the global positioning system and mobile-phone data transmission. The drifters worked well and the accuracy was reasonable (std dev. 40 m). Five drifters were used to map ice kinematics in a 20 km size array in the coastal drift-ice zone. The study included periods of onshore motion with ridge formation, and alongshore motion with narrow shear lines. The motion of ice largely occurred in short pulses between which the field stood nearly still. The level of ice speed was much less than that of free drift, while the deformation field was more uniaxial due to the presence of the solid boundary. Drift-ice strength was estimated as 4×10^4 N m^{-2}. Large deformation rates of up to 2% h^{-1} were observed.

1. INTRODUCTION

Drift ice is a granular medium consisting of ice floes. Each floe performs its own individual trajectory or drift path, and on scales much larger than the floe size the picture of motion resembles the motion of a continuum. In drift-ice kinematics, the approach may be based on continuum mechanics (e.g. Hibler and others, 1974; Leppäranta, 1981) or purely on statistics (e.g. Thorndike, 1986). In the former case, kinematics data are used to learn about the laws of drift-ice dynamics and to perform ice-dynamics model calibrations, while in the latter case kinematics data are used to extract the relevant parameters of the underlying stochastic processes. The present work is based on the continuum approach.

Drift-ice kinematics can be mapped by two different techniques. First, measurements are made with various types of drifters which track the trajectory of the floe upon which they have been deployed. These methods include manned stations, ARGOS buoys (Thorndike and Colony, 1982), laser geodimeters (Hibler and others, 1974; Leppäranta, 1981) and microwave transponder systems (Leppäranta and Hibler, 1987). Secondly, imaging remote-sensing methods are used to determine the field of floe displacements from sequential data. In particular, imaging radars serve this purpose well because of their high resolution and weather and darkness independence. For satellite-borne synthetic aperture radar (SAR), ice kinematics has been one of the most useful sea-ice products (e.g. Sun, 1996). Coastal radar stations were introduced for ice monitoring in Hokkaido, Japan, in the late 1960s and are able to map the 100 km zone adjacent to the coastline (Tabata, 1972). The drifter method provides velocity time series, while the sequential imaging method produces displacement fields or mean velocities over longer time intervals. While coastal radars offer a compromise, they have a limited spatial range.

In the Baltic Sea, drift-ice kinematics has been widely studied since the 1970s. The motivation has been to construct sea-ice models and to develop ice-forecasting methods for winter shipping (Leppäranta, 1981). First, the Decca Navigator system and ship radars were utilized (Omstedt and others, 1974). For more accurate data, laser geodimeter and microwave transponder systems were used by Leppäranta (1981). Subsequently, ice-displacement fields were extracted and analyzed from airborne and satellite SAR images (Leppäranta and others, 1998). Recently, the coastal zone has attracted more attention since the ice motion there changes rapidly and it is uncertain how well present models can represent the dynamics problems there.

Field experiment ZIP-97 (Zooming of Ice Physics, 1997) was carried out from 5 to 21 March 1997 in the Bay of Bothnia, the northernmost basin of the Baltic Sea (Haapala and Leppäranta, 1997). The main objective was to study the downscaling of ice physics from the basin-wide scale to the local scale. A large dataset was also collected from the coastal zone, as the experimental base was on the island of Hailuoto at the fast-ice boundary. Zhang (in press) has compared the data with the outcome of a sea-ice dynamics model. This paper presents the results of the ice-kinematics data analysis. A new drifter system based on the global positioning system (GPS) and data transmission via a radio modem is introduced (Stipa and Haapala, 1997). It effectively supersedes its precursors by offering high-resolution mapping capability with low-cost drifters.

2. EXPERIMENT ZIP-97

The Bay of Bothnia has a surface area of 37 000 km^2 and mean and maximum depths of 43 and 147 m, respectively. In the north, there is a wide archipelago, with Hailuoto at 65° N being the largest island. The water salinity is very low (3–4‰), with a halocline (and pycnocline) at 30–40 m depth. The brackish-water ice of the Baltic Sea has a structure similar to sea ice. It forms fast ice in coastal areas and skerries, and drift ice further out. The amount of ridged ice is 10–50% of the total ice volume; typical ridge thicknesses are 5–15 m. In the coastal drift-ice zone, the ice mechanics is strongly affected by the presence of the fixed (fast-ice)

https://doi.org/10.3189/172756401781818789 Published online by Cambridge University Press

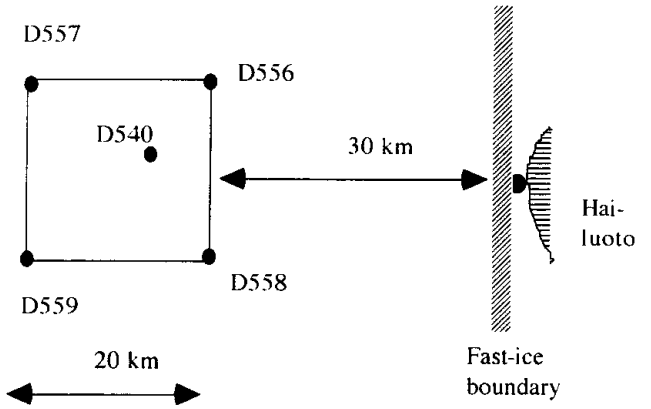

Fig. 1. The deployment of the drifter array (drifters coded as D557, etc.) in the coastal drift-ice zone.

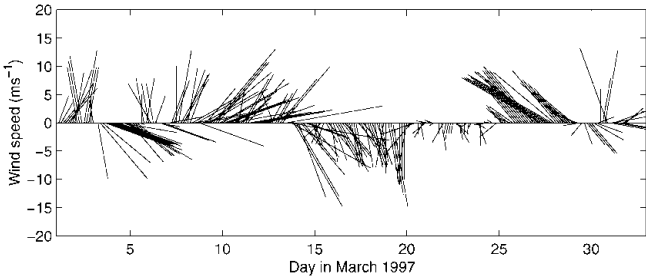

Fig. 2. The wind velocity in ZIP-97 shown as a vector time series. The vectors are averages of the wind at the lighthouses Marjaniemi (at the base) and Kemi 1 (70 km north).

boundary. This zone is 20–50 km wide, and across it the ice velocity typically undergoes large changes with heavy ice deformation, and the ice conditions may change significantly over short time- and space scales. The sea around Hailuoto is shallow (5–20 m), and the fast-ice boundary is usually (as in 1997) at its outer shore. Ridges form off the island and may ground in places, so the near-shore zone is more stable than the pack ice further out. Sometimes a slip line forms at the edge of this zone.

The ZIP-97 experiment addressed three scales (Haapala and Leppäranta, 1997): (i) basin-wide (100 km) mapping by satellites and helicopter reconnaissance; (ii) intermediate-scale (10 km) mapping by satellite and airborne systems and a drifter array; and (iii) local-scale (10 m) in situ surveys. The second scale is examined in the present work. A new GPS drifter system has been constructed (Stipa and Haapala, 1997) using ordinary (not differential) GPS. The data stream from a GPS receiver is directly connected to a radio modem for the data transmission. The power consumption, which is determined by the GPS receiver, was a major constraint on the drifter design. In order to secure an operating life of 3 weeks, a 200 Ah 12 V lead acid gel battery was used. The drifter shell was made of 400 mm acid-proof steel sewage tubing with a 3 mm wall thickness, and the total weight of one drifter was about 150 kg. Five drifters were deployed in a 20 km square from 5 to 7 March in the ice pack at distances 20–40 km from the fast-ice boundary (Fig. 1). The sea depth was 20–50 m. Close to the drifter array, the fast-ice boundary was directed northwards (the direction of the major axis of the Bay of Bothnia is 30° clockwise from the north).

There were inherent problems in the cellular radio transmission due to bad weather. Almost all data were received for the closest drifters, but there are several missing observations for the furthest drifter. In good weather conditions, the signal should be received at about 100 km distance. Before the end of the experiment, drifter D557 ceased to transmit data. The ice itself also caused problems: drifters D540 and D556 were encapsulated in a newly formed ridge and could not be dug out. In the summer, however, all three of these drifters were recovered from the coastal waters of the basin in their original shape except that the antennas had been crushed. The data collection was successful from 5 to 14 March, although data gaps occur after that time.

To study mesoscale ice dynamics, a high accuracy is needed. For example, to have 2 h temporal resolution and 0.01 m s^{-1} velocity resolution, the positional accuracy must be better than 36 m. The accuracy was examined by recording a fixed position at the base. All data were within a circle of diameter 150 m, giving an estimate of $\sigma \approx 40$ m for the standard deviation of the position error ($\pm 2\sigma$ is then within about 150 m). Consequently, the standard deviation becomes 56.4 m for displacements and 80 m for spatial differential displacements. Differences in consecutive observations were usually much less; in most cases, the change was <2.5 m at the 10 min sampling rate. The inertial time-scale of the thin Baltic Sea ice is $T_I \sim 10^3$ s (see section 3.1) and it would be good to have a much shorter sampling interval if only the measurement accuracy were still better. However, sudden large shifts did occur, and taking the GPS error as white noise with 40 m standard deviation gives a safe error estimate when a drifter is in a fixed location.

3. RESULTS

3.1. Overall evolution of the ice field

Information on the ice conditions was obtained from routine ice charts of the Finnish Institute of Marine Research as well as from ZIP-97 ice surveys. At the beginning of March, the basin was almost totally ice-covered, and the size of the drift-ice field was 180 km in the north–south direction and up to 120 km in the east–west direction. The ice had been packed more toward the east and north coasts by the prevailing westerly winds. The thickness of the coastal fast ice was 0.4–0.8 m, and in the north the undeformed ice in the drift-ice field was 0.2–0.5 m thick. Several deformation events had occurred during the winter, so the amount of ridged ice was large. During a northerly storm from 15 to 18 March, the ice on the eastern side of the basin was compact and weakly moving southward, while further out there was a sharp shear line with more loose ice drifting much faster in the west.

Wind data were available at the Finnish Meteorological Institute for the lighthouse stations Kemi 1 and Marjaniemi and were averaged for a representative wind field (Fig. 2). The weather was windy and the ice conditions changed much in the basin. The wind speed was usually >5 m s^{-1}, with strong winds (>15 m s^{-1}) occurring on the 9th, 12th, 14th and 19th. From 5 to 13 March, southerly and south-westerly winds drove the ice northeastwards, opening a wide lead in the south and forming new ridges off the Finnish coast in the north. Two major ridging events occurred on 12 and 14 March. Then the wind direction turned northerly, and the ice moved back southwards, opening a flaw lead at the northern fast-ice boundary. Due to the cold weather, the

https://doi.org/10.3189/172756401781818789 Published online by Cambridge University Press

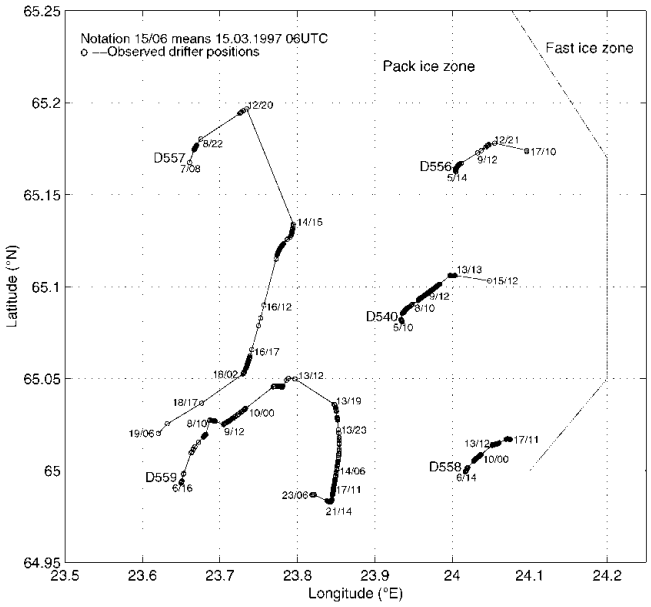

Fig. 3. The GPS drifter trajectories, 5–23 March 1997. The drifter labels are shown at the beginning of each track.

lead froze over, and at the end of the experiment the basin was fully ice-covered again.

The path of the drifter array is shown in Figure 3. Between 7 and 12 March the southwesterly winds forced the array to the northeast, with compression occurring toward the fast-ice boundary. The ice motion was directed to the right from the wind, as expected, but was also affected by the basin geometry. Then the northerly wind drove drifters D557 and D559 south, while only small changes occurred in the behaviour of the other drifters. A large shear strain therefore resulted in the array. In fact there were at least two marked shear lines in the coastal boundary zone: one within the drifter array about 30 km from the fast-ice boundary, and the other 10 km further out.

The raw 10 min data were used for the first look analysis. For further analyses, the gaps were filled by linear interpolation, and the time series were low-pass filtered with the filter transition band of 6–8 cpd (cycles per day) using the Kaiser filter. The cut-off band was chosen to make the noise level lower than the signal and to ensure that sudden shifts created by the GPS system were sufficiently smooth. The GPS noise is not necessarily Gaussian, which may affect the features of the filtered time series. There are no significant tides in the Baltic Sea; inertial oscillations are often found, but they are not fully resolved by the present filter. The filtered records were resampled at 2 h intervals to make the Nyqvist frequency equal to the filter cut-off. This low-pass filtering with cut-off reduced the noise level to 10 m.

Unfortunately, a serious outlier problem was found. In seven cases, remarkably rapid displacements, on the order of 1 km per 10 min, were recorded, but they are considered questionable. A careful examination showed that the most likely explanation is the following. Occasionally, GPS errors may become quite large in recording sequential shifting positions, i.e. there is inertia in the system to determine whether a drifter has been displaced or not. Such rapid shifts have not previously been reported from this basin. Distributed over a 4 h filtering period, a 1 km displacement averages to 42 m which is the standard deviation for the positioning of a fixed position.

3.2. Ice drift

The equation of motion of drift is written (e.g. Leppäranta, 1998):

$$\rho H\left[\frac{\partial \boldsymbol{u}}{\partial t}+\boldsymbol{u}\nabla\boldsymbol{u}+f\mathbf{k}\times\boldsymbol{u}\right]=\nabla\sigma+\tau_{\mathrm{a}}+\tau_{\mathrm{w}}-\rho Hg\nabla\xi\,, \tag{1}$$

where ρ is ice density, H is ice thickness, $\boldsymbol{u}$ is ice velocity, t is time, f is the Coriolis parameter, $\mathbf{k}$ is the unit vector vertically upward, σ is ice stress, τ_{a} and τ_{w} are the tangential stresses of air and water on ice, g is the acceleration due to gravity, and ξ is the sea-surface elevation. The governing terms in the dynamics of the thin Baltic Sea ice are the internal friction of the ice and the air and water stresses. A natural inertial time-scale becomes $T_{\mathrm{I}}\sim\tau_{\mathrm{a}}/(\rho HU)$, where U is the ice-velocity scale. For $U\sim 0.1\,\mathrm{m\,s^{-1}}$, we have $T_{\mathrm{I}}\sim 10^{3}\,\mathrm{s}$.

An extreme is the free-drift case. The internal friction and advection are neglected and then the stationary solution of the free-drift velocity $\boldsymbol{u}_{\mathrm{F}}$ is (e.g. Leppäranta, 1998):

$$\boldsymbol{u}_{\mathrm{F}}=\boldsymbol{u}_{\mathrm{Fa}}+\boldsymbol{u}_{\mathrm{w}}\,, \tag{2}$$

where $\boldsymbol{u}_{\mathrm{Fa}}$ is the wind-driven free-drift velocity and $\boldsymbol{u}_{\mathrm{w}}$ is the water velocity beneath the surface boundary layer. The former part is obtained by contraction (wind factor α) and rotation (clockwise deviation angle θ). In the Baltic Sea free-drift conditions, $\alpha\approx 2.5\%$ and $\theta\approx 30^{\circ}$ (Leppäranta and Omstedt, 1990). For moderate and strong winds, the wind-driven contribution dominates in the Baltic, $\boldsymbol{u}_{\mathrm{F}}\approx\boldsymbol{u}_{\mathrm{Fa}}$.

With plastic internal ice friction, the one-dimensional solution is (Hibler, 1986):

$$\boldsymbol{u}^{2}=\max[0,(\tau_{\mathrm{a}}-P^{*}H/L)/(\rho_{\mathrm{w}}C_{\mathrm{w}})]\,, \tag{3}$$

where P^{*} is the compressive strength of the ice, L is the wind fetch, ρ_{w} is water density and C_{w} is the ice–water drag coefficient. Thus the ice fails as soon as $\tau_{\mathrm{a}}L>P^{*}H$. In the present case under westerly wind the ice generally moved when the wind speed was $>10\,\mathrm{m\,s^{-1}}$ ($\tau_{\mathrm{a}}>0.2\,\mathrm{N\,m^{-2}}$), and with $L\approx 100\,\mathrm{km}$ and $H\approx 0.5\,\mathrm{m}$ we have $P\approx 4\times10^{4}\,\mathrm{N\,m^{-2}}$ which is close to the value of $3\times10^{4}\,\mathrm{N\,m^{-2}}$ observed earlier in the same basin (Leppäranta and others, 1998). Thus a natural length scale is $L\sim P^{*}h/\tau_{\mathrm{a}}$ which is about 40 km for the present maximum wind speed of $15\,\mathrm{m\,s^{-1}}$.

In the coastal zone of the drifting ice pack, the free-drift model is usable for offshore winds, but becomes seriously biased when the wind has an onshore component (Leppäranta, 1998). In the coastal zone, the wind-factor level is an indication of how strongly the internal friction of the ice is resisting the motion. The result for an onshore (within $\pm30^{\circ}$) wind direction agrees with Equation (3) and ends up with a motionless condition where the wind stress can no longer overcome the yield strength of the ice (Leppäranta and Hibler, 1985). If the wind has an onshore component but is directed onshore $<60^{\circ}$, there is an adjustment of the ice-thickness distribution so that a shear flow develops parallel to the fast-ice boundary. The ice velocity is $u_{\parallel}=\alpha^{*}u_{\mathrm{a}}$, where α^{*} is a coefficient ($0<\alpha^{*}<\alpha$) depending on the shear strength of the ice and wind direction.

For the present data, the ice velocities were obtained from the positions by first-order differencing. Assuming that the position error is white noise with a sampling interval Δt and variance σ^{2}, the variance spectrum of a velocity component is

$$p(\omega)=(\sigma/\Delta t)^{2}\times[1-\cos(\omega\Delta t)]/\pi,\ 0\le|\omega|\le\pi\,, \tag{4}$$

where ω is frequency. The observed ice-velocity spectra were

https://doi.org/10.3189/172756401781818789 Published online by Cambridge University Press

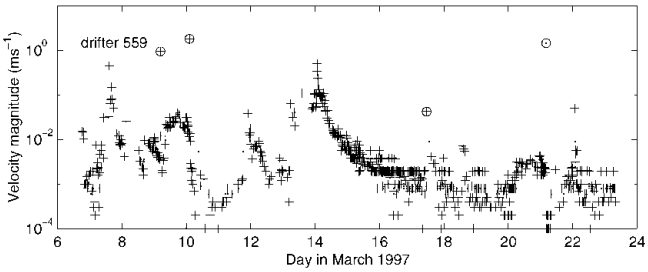

Fig. 4. Observed velocity time series of drifter D559. The raw 10 min data are presented as crosses; the circled points are classified as outliers due to the GPS errors. The straight line equal to 0.01 cm s^{-1} shows a conservative uncertainty limit.

quite flat for frequencies of >2 cpd and hit the noise level at 5–10 cpd frequencies. Consequently the filtered data (6–8 cpd transition band) were used for further kinematics analysis. The total standard deviation is $\sqrt{2}\sigma/\Delta t$ which is 94 mm s^{-1} in the raw data ($\Delta t = 10$ min) or 3.9 mm s^{-1} in the filtered data.

From zero to 2 cpd the velocity spectra were red. Closer to the fast-ice boundary, the red portion became weaker. Ice speeds of >0.05 m s^{-1} were observed only four times, on 7, 13–14, 17 and 22 March, even though the wind speed was usually >5 m s^{-1}. These events lasted about half a day each. The first and second cases were connected with ridging events under southwesterly winds, while the third case occurred during the northerly storm.

The northerly wind caused a slight offshore component in the ice drift in the north, but further south the direction of the coastline turned toward the wind direction. The coast provided a barrier for the drift ice, so the velocity did not approach the free drift, but there was a long shear line further out, beyond which the free-drift state appeared. The ice resistance was consequently dominated by its compressive strength, and a good estimate for the shear strength of the ice was not obtained. Over the next 3 days, the freely drifting ice continued south and cracks appeared in the compact coastal zone.

The time series of the drifter D559 velocity is shown in Figure 4. The ice velocity was usually very low, well below 0.01 m s^{-1}, which in fact is zero within the given accuracy. The movement took place in short pulses of not more than 12 h. The only exception started in the evening of 14 March, when the velocity peaked sharply at 0.5 m s^{-1} and the spin-down lasted >1 day. Such high speeds are occasionally observed in the Baltic under very strong winds. Also shown are a few outliers resulting from GPS errors as discussed above. The velocity outcome in the drifters was well correlated, but closer to the fast-ice boundary the levels were lower. The maximum speed was about 0.05 m s^{-1} for drifters D556 and D558 and 0.1 m s^{-1} for drifter D540.

It is clear that the drift velocity was different from the free-drift case (Fig. 5). With increasing wind speed, however, the ice speed approached the free-drift level. This is expected for a plastic system where drag forces scale with squared velocities but the internal friction is strain-rate (or coastal-velocity) independent. In the other drifters, there was a similar tendency but not so strong as for drifter D559. For lower wind speed, the ice speed was close to the measurement noise level. Also, with increasing wind speed the angle between the ice and wind velocities converged toward 40–45° while the free-drift value was 30° in the Baltic. This difference is due to the geometry in the dynamics of the ice field, favouring the main axis of the basin, because the width of the basin is only about twice the length scale $L \sim P^* h/\tau_a$ of compact Baltic drift ice.

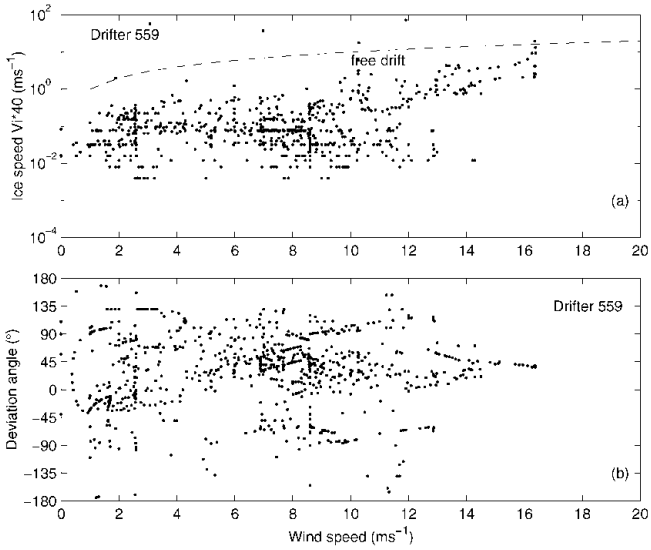

Fig. 5. Based on drifter D559 are shown: (a) the wind factor equal to the ratio of ice speed to wind speed, the dashed line illustrating the theoretical free-drift value; and (b) deviation angle (clockwise angle from wind vector to ice-velocity vector). Free-drift value is about 20° for wind speed >10 m s^{-1}.

3.3. Ice deformation

Deformation of the ice field is obtained from the velocity gradient:

$$\varepsilon = [\nabla \boldsymbol{u} + (\nabla \boldsymbol{u})^{\mathrm{T}}]/2, \omega = (\partial v/\partial x - \partial u/\partial y)/2\,, \qquad (5)$$

where ε is the strain-rate tensor, ω is the vorticity, and u and v are the x and y components of the ice-velocity vector $\boldsymbol{u}$ (e.g. Hibler and others, 1974; Leppäranta, 1998). Strain rate has two principal axes with values ε_1 and ε_2, $\varepsilon_1 > \varepsilon_2$, and furthermore their sum equals the divergence of the flow and their difference gives twice the maximum rate of shear in the deformation. The filtered velocities were used to estimate the deformation, and the standard deviation became approximately $2\sigma/(l\Delta t) \approx 1.0 \times 10^{-3}$ h^{-1}, where $l = 20$ km is the size of the measurement array.

The area of the drifter array decreased significantly during the experiment (Fig. 6). In the beginning it was 310 km^2, and it decreased to 200 km^2 on 17 March before

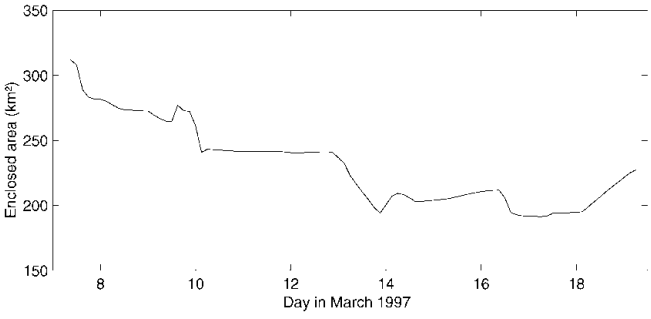

Fig. 6. Evolution of the drifter array area during the period of the experiment.

https://doi.org/10.3189/172756401781818789 Published online by Cambridge University Press

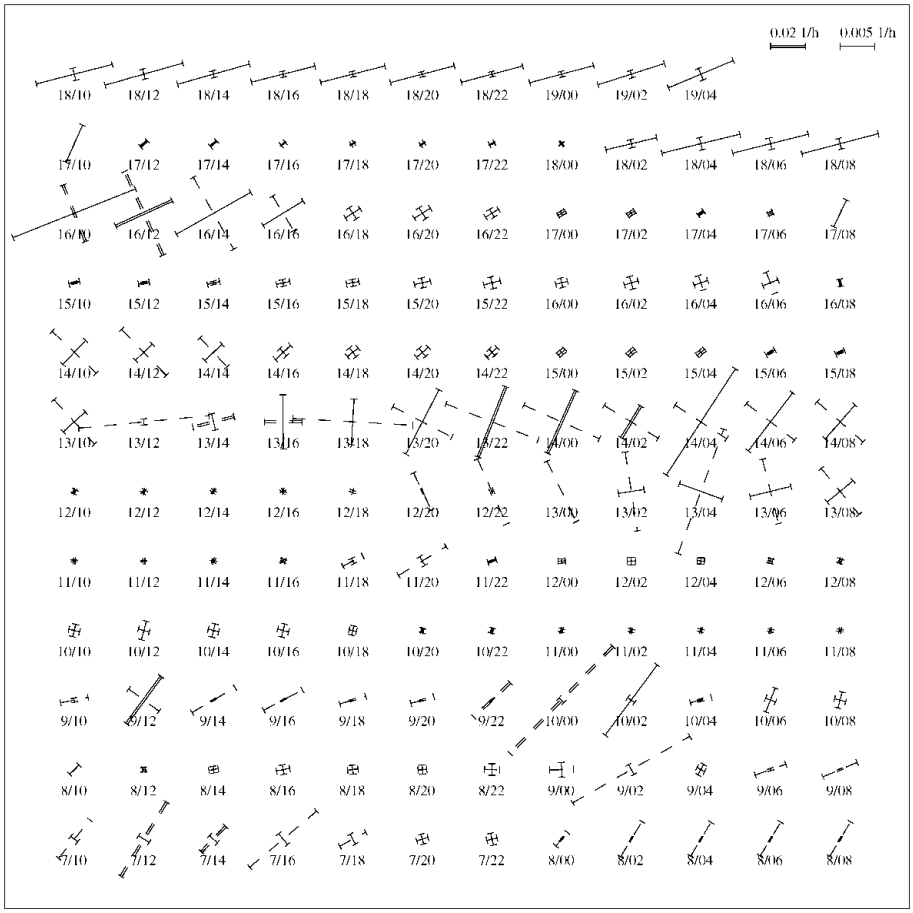

Fig. 7. Principal-axis presentation of the strain-rate tensor at 2 h time intervals based on the filtered data. North is up. The notation 10/15 means 10 March 1997, 1500 h UTC. Solid lines mark dilatation, and dashed lines mark contraction.

starting to increase again. Since the initial ice compactness was about 1.0, this means that the ice thickness must have increased by 50% within the area of the array.

The time series of the principal-axis presentation of the strain rate illustrates the physical deformation of the drifter array (Fig. 7). Half of the time, the deformation level was close to the measurement noise level. It is seen that often the strain was nearly uniaxial. In two cases there was a biaxial strain period of about half a day: (1) 13 March, 1800 h to 14 March, 0800 h, and (2) 16 March, 1000–1800 h. The uniaxial strain equals convergence and also twice the maximum shear strain. In the biaxial cases, the signs of the principal-axis values were opposite, which gives smaller convergence and larger shear. Whether contraction or dilatation, there was a dominant direction, although this varied over different cases. The direction comes from the wind and coastline orientation. Also it is seen that major deformation events lasted about half a day, as was also the case for the motion events. The reason for this is not known, but the forcing and the evolution of ice strength lie in the background.

From 7 to 9 March, there were more-or-less onshore convergence cases, with ridge formation being observed. On 14 March, there was substantial deformation in both principal-axis directions, with contraction along one axis and dilatation along the other. The contraction axis was again onshore and resulted in the second ridging episode during the experiment. When the wind shifted north after 13 March, deformation was at first weak. Subsequently, on 18 March, nearly uniaxial dilatationtook place. The ice opened up, with cracking parallel to the coastline; the northerly wind tends to open the ice since, via the Coriolis effect, the ice drifts 20–30° to the right of the wind direction.

The directions of the principal axes were mainly northeast and northwest. That is, the geometry of the whole basin rather than the direction of the local fast-ice boundary determined them. The length scale of deformation being comparable to the size of the basin, the geometry plays a major role. Like the strain rate, vorticity was also very low except for short intensive periods (Fig. 8). There was a negative tendency from 9–10 March with a peak of $-0.1^\circ\,h^{-1}$. The vorticity was close to zero at this time, but otherwise peaked at $0.2^\circ\,h^{-1}$ late on 11 March. The magnitude of vorticity appears to be much less than the rate of shear in the present data, which is likely due to the direction of the forcing with respect to the coastline orientation.

Compared with results from the central basin of the Bay of Bothnia (Leppäranta, 1981), the main differences are that the proportion of (nearly) uniaxial strain cases is larger and that the level of large deformation rates is larger ($2\%\,h^{-1}$ compared to $<1\%\,h^{-1}$ in the central basin). Both these features can be explained by the presence of the coastline, which limits the deformation possibilities and which introduces large spatial changes for the plastic ice flow at the fixed boundary.

4. CONCLUSIONS

A sea-ice dynamics experiment ZIP-97 was performed in the

https://doi.org/10.3189/172756401781818789 Published online by Cambridge University Press

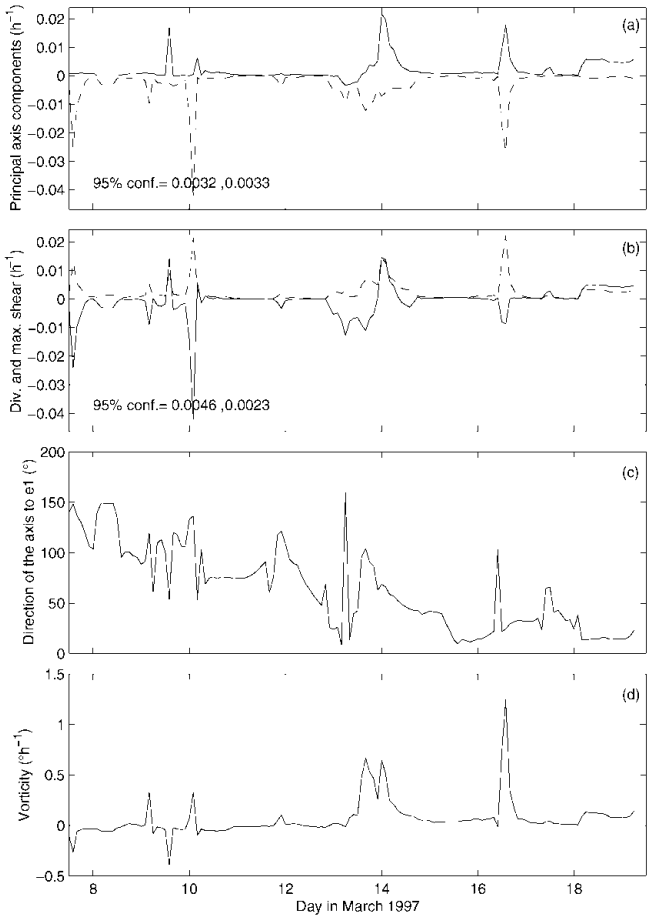

Fig. 8. The time series of the deformation of the drifter array based on the filtered data: (a) principal strain rates $\varepsilon_1 > \varepsilon_2$; (b) divergence (solid line) and maximum rate of shear (dashed line); (c) direction of the first principal axis; and (d) vorticity.

Bay of Bothnia in March 1997, using a new type of drifter based on GPS and a radio-modem data transmission. They worked well and the accuracy was good (std dev. 40 m). The basin size was about 250 km × 150 km, and the size of the drifter array was a 20 km square located 20–40 km from the fast-ice boundary. The data collection lasted 2 weeks. In 1997 there was still artificial dithering noise in the GPS, but at the time of writing it is claimed that the noise has been removed, which would much improve the measurement accuracy of our drifters.

The study period included onshore motion with ridge formation, and alongshore motion with narrow shear lines occurring. The motion of the ice mostly occurred during short pulses (<12 h) between which the motion field was approximately stationary. The level of ice speed was much less than the theoretical free-drift speed, being <0.1 m s^{-1}. With increasing wind speed, the ice/wind velocity ratio started to increase toward the free-drift speed as expected for a plastic ice field. The direction of ice drift was significantly affected by the geometry of the basin. Based on the coastal frictional effects, the strength of the compact drift ice was estimated at 4×10^4 N m^{-2}.

The deformation field was more uniaxial than that in the central basin due to the presence of the solid boundary. The most common principal-axis orientation corresponded to the axes of the basin. For half of the time, the deformation was below the measurement noise level, and large deformation rates, up to 2% per hour, lasted <12 h. Vorticity was lower than the rate of shear. The coastal-zone deformation differs from the central basin deformation in its larger rates, pulsed structure and greater uniaxiality.

ACKNOWLEDGEMENTS

C. A. Geiger and R. Massom are thanked for most valuable comments on the manuscript. The work described here was supported by the European Commission, DG-XII, through the Marine Science and Technology program 1994–98 (MAST III) under contract MAS3-CT95-0006. The participating institutes in this joint project, entitled ICE STATE, are the Helsinki University of Technology, the Nansen Environmental and Remote Sensing Centre, Norway, the Scott Polar Research Institute, U.K., the University of Helsinki and the University of Iceland.

REFERENCES

Haapala, J. and M. Leppäranta. 1997. ZIP-97 overview. *In* Haapala, J. and M. Leppäranta, *eds. ZIP-97 Data Report*. Helsinki, University of Helsinki. Department of Geophysics, 7–25. (Report 37.)

Hibler, W. D., III. 1986. Ice dynamics. *In* Untersteiner, N., *ed. Geophysics of sea ice*. London, etc., Plenum Press, 577–640. (NATO ASI Series B: Physics 146.)

Hibler, W. D., III, W. F. Weeks, A. Kovacs and S. F. Ackley. 1974. Differential sea-ice drift. I. Spatial and temporal variations in sea-ice deformation. *J. Glaciol.*, **13**(69), 437–455.

Leppäranta, M. 1981. On the structure and mechanics of pack ice in the Bothnian Bay. *Finn. Mar. Res.* 248, 3–86.

Leppäranta, M. 1998. The dynamics of sea ice. *In* Leppäranta, M., *ed. Physics of ice-covered seas. Vol. 1.* Helsinki, University of Helsinki Press, 305–342.

Leppäranta, M. and W. D. Hibler, III. 1985. The role of plastic ice interaction in marginal ice zone dynamics. *J. Geophys. Res.*, **90**(11), 11,899–11,909.

Leppäranta, M. and W. D. Hibler, III. 1987. Mesoscale sea ice deformation in the East Greenland marginal ice zone. *J. Geophys. Res.*, **92**(C7), 7060–7070.

Leppäranta, M. and A. Omstedt. 1990. Dynamic coupling of sea ice and water for an ice field with free boundaries. *Tellus*, **42A**(4), 482–495.

Leppäranta, M., Yan Sun and J. Haapala. 1998. Comparisons of sea-ice velocity fields from ERS-1 SAR and a dynamic model. *J. Glaciol.*, **44**(147), 248–262.

Omstedt, A., T. Thompson and I. Udin. 1974. *Havsisundersökningen i Bottenviken vintern 1974*. Stockholm, Winter Navigation Research Board. (Res. Rep. 8.)

Stipa, T. and J. Haapala. 1997. GPS-drifters. *In* Haapala, J. and M. Leppäranta, *eds. ZIP-97 Data Report*. Helsinki, University of Helsinki. Department of Geophysics, 59–67. (Report 37.)

Sun, Y. 1996. Automatic ice motion retrieval from ERS-1 SAR images using the optical flow method. *Int. J. Remote Sensing*, **17**(11), 2059–2087.

Tabata, T. 1972. Radar network for drift ice observations in Hokkaido. *In* Karlsson, T., *ed. Sea Ice, Proceedings of an International Conference, 10–13 May 1971, Reykjavík, Iceland*. Reykjavík, National Research Council, 67–71.

Thorndike, A. S. 1986. Kinematics of sea ice. *In* Untersteiner, N., *ed. Geophysics of sea ice*. London, etc., Plenum Press, 489–549. (NATO ASI Series B: Physics 146.)

Thorndike, A. S. and R. Colony. 1982. Sea ice motion in response to geostrophic winds. *J. Geophys. Res.*, **87**(C8), 5845–5852.

https://doi.org/10.3189/172756401781818789 Published online by Cambridge University Press